

Identifying Chaotic Behavior in Non-linear Vibration Energy Harvesting Systems

M. Mohammadpoura, S. M. Mohsen Modarres-Gheisari, P. Safarpour,
R. Gavagsaz-Ghoachani, M. Zandi*

Faculty of Mechanical and Energy Engineering, Shahid Beheshti University, Tehran, Iran.

Received Date 16 November 2020; Revised Date 16 December 2020; Accepted Date 20 December 2020

*Corresponding author: M_zandi@sbu.ac.ir (M. Zandi)

Abstract

Large amplitude inter-well oscillations in bi-stable energy harvesters have made them a proper energy harvesting choice due to a high energy generation. However, the co-existence of the chaotic attractor in these harvesters could essentially decrease their efficiency. In this work, an algorithm for detecting chaos in bi-stable energy harvesters based on a data-gathering algorithm and estimating the largest Lyapunov exponent is investigated. First, a simple model of axially-loaded non-linear energy harvesters is derived. This model is derived using the Euler-Bernoulli beam theory and the Assumed Mode method considering the Von-Karman non-linear strain-displacement equation. The harvester's numerical simulation results are used in order to test the algorithm's efficiency and accuracy in identifying the chaotic response. The results obtained show the algorithm's success in detecting chaos in such systems with a minimum possible calculation cost. The effect of noise on the algorithm's performance is also investigated, and the results obtained show an excellent robustness of the algorithm to noise. It can diagnose the harvester's chaotic or harmonic behavior with noise-contaminated data with 10% noise density. The comparison between this algorithm and the Wolf's method show a relatively less computation time (up to 80%) to detect chaos with a reasonable accuracy.

Keywords: Energy Harvesting, Bi-stability, Chaos, Largest Lyapunov Exponent.

1. Introduction

In the last decades, the aim of mitigating carbon emission and fossil fuels' environmental effects has encouraged the use of renewable energies [1]. There are different types of renewable energies including but not limited to wind, solar, geothermal, and biomass [2]. More recently, harvesting the vibration energy as a sustainable renewable source for power has also been an emerging idea, attracting the researchers' attention [3]. At first, the linear energy harvesters have been investigated by many researchers according to their simple modeling design and fabrication; however, after some years, it has been shown that the linear energy harvesters have some significant disadvantages [4]. In the recent years, the use of non-linear energy harvesters has been proposed by many researchers in order to overcome the drawbacks of the linear harvesters such as limited bandwidth and efficiency [5].

There are two major non-linear energy harvester types, which are the Duffing-type oscillators with mono-stability and bi-stability [6]–[8]. Among different non-linear energy harvesters, many

researchers have investigated the bi-stable ones in order to use the non-linear large amplitude oscillations to increase the energy harvesting efficiency [9]. The large amplitude inter-well oscillation in bi-stable harvesters leads to a high-performance energy harvesting, making the bi-stable ones a proper energy harvester [10].

In 2008, McInnes *et al.* [11] proposed using the stochastic resonance in a bi-stable energy harvester. Their results showed that adding harmonic excitation to the primary noise excitation can significantly increase the harvested energy. In 2009, Cottone *et al.* [12] induced the post-buckling behavior in a cantilever beam using the electromagnetic force and used it as a bi-stable energy harvester. Their investigations showed that using a bi-stable energy harvester can increase the harvested energy between 400% to 600% compared with a similar linear counterpart. Naseer *et al.* [8] have done a comparative study of bi-stable energy harvesters under fluid vortex induction with the mono-stable ones. Their result indicated that the bi-stable energy harvester

significantly outperformed in slow wind speeds. In the moderate and high wind speeds, it performs almost better than the mono-stable energy harvesters.

Mann and Owen [13] have studied the bi-stable energy harvester under harmonic excitation with varying frequency to capture the frequency response system. The numerical and experimental results of their investigation showed that escaping from a potential well can widen the frequency bandwidth of the harvester. Stanton *et al.* [14] have investigated the bi-stable energy harvester's behavior using the harmonic balance method. In their research work, they achieved a closed-form response to design the harvester's coupling factor to tune the high energy orbit's stability threshold.

Following the research in bi-stable energy harvesters, Panyam *et al.* [15] have studied the bi-stable energy harvester's response. Using numerical integration, they achieved the system's bifurcation diagram according to the excitation frequency (frequency response). Their investigation shows many different non-linear phenomena such as cyclic folding, 1T, 3T, 5T windows of periodic responses, chaotic response, and boundary crisis in the bi-stable energy harvester [15]. They showed that chaos in the bi-stable energy harvester's response could drastically decrease the harvested energy.

In order to overcome this issue, some researchers have investigated chaos control in the bi-stable energy harvesters [16]–[18]. Kumar *et al.* [16] have studied the chaos control in the bi-stable energy harvester using Linear Quadratic Regulators (LQR). Utilizing Ott, Grebogi, Yorke (OGY) [19], the control force successfully forced the system to oscillate in a large amplitude orbit rather than a co-existent chaotic attractor. Huynh *et al.* [17] have presented a controlled vortex-induced bi-stable energy harvester. They derived the governing equations of motion, and then designed a controller using the OGY chaos control theory to create a stable orbit. The numerical and experimental studies have shown that the designed control system properly transfers the harvester's behavior from chaotic to stable large-amplitude orbit.

The experimental implementation of chaos control in bi-stable energy harvesters requires a method for chaos detection from time series measured data [20]. The chaos control methods always use energy in the actuators [21]. This energy consumption would decrease the efficiency of the harvester. If the chaos control method is implemented without chaos detection, the control loop may consider higher period orbits or noise as

chaos and consume unnecessary energy. Due to this, the use of chaos detection algorithm is inevitable. There are several ways available for detecting chaos from time-series data including Largest Lyapunov Exponent (LLE), Kolmogorov entropy, and correlation dimension. Harris *et al.* [22] have used the multi-scale entropy method and the "0-1" test in order to detect chaos in a bi-stable beam. The results of their work showed that both methods could detect chaos with an acceptable efficiency. However, sensitivity to selecting algorithm parameters in correlation dimension and Kolmogorov entropy made LLE a more proper method [23].

Wolf [23] has presented an algorithm to detect chaos from the time-series experimental data. Although calculating LLE is the most reliable method used for identifying chaos, its main drawbacks are the massive amount of data required to be processed and the calculation costs [24]. This cost could bring some main difficulties. Most of the energy harvesting systems are designed in micro-scales. At that scale, the processing power of the processors and the available memories are very low. During the calculation time, the disadvantages of the chaotic behavior are still there. Secondly, sometimes the chaotic behavior is temporal, and with lag in the detection, we may pass the chaotic regime and try to control the thing that no longer exists. Furthermore, the algorithm is sensitive to the external noise on the dataset.

The algorithm proposed by Wolf has then been improved by many researchers [25]–[27] in order to solve the sensitivity to noise and extended run time. Rosenstein has proposed an m-dimensional gridding technique using the mean of the different LLE estimations to decrease the effect of external noise [25], leading to a robust but complex algorithm. Mehdizadeh [28] has proposed using the mean distance of points in the initial point neighborhood instead of the closest point. The proposed algorithm is robust to noise and accurate, and has a longer run time than the Rosenstein's algorithm. Zhou *et al.* [26], [27] have presented a much more fast algorithm. In that algorithm, they used the distance between two pseudo-orbits in the attractor's phase space and calculated the evolution of this distance concerning time. This algorithm is fast but it requires to have the exact model of the system. In real applications of energy harvesting, having the exact non-linear harvester model is a relatively challenging issue. Besides, the model's parameters can vary during the work-life of the harvester due to depreciation.

The novel, simple, non-linear Model for Axially Loaded Energy Harvesters (MALEH) is presented in this paper. In MALEH, despite Masana and Daqaq [29], the beam section's axial displacement is considered negligible, and a Von-Karman Strain is used to model the system. This assumption made the harvester model simple without a significant loss of accuracy and generality, helping the design chaos controllers. A new Modification of Wolf's Method (MWM) is utilized in this work in order to calculate LLE of a bi-stable piezoelectric energy harvester. MWM is implemented using the minimum possible randomly selected data points from the complete dataset. Unlike the Wolf's algorithm, the system's embedding dimension is also set up to be as equal as the system dimensions. Although utilizing the minimum data points and embedding dimension could affect the accuracy of the calculated LLE, the results obtained show that a proper detection of chaos is possible with this minimum embedding dimension. Moreover, the piezoelectric elements' output voltage is used as the time series data, so there is no need to use an extra sensor, which may cause extra cost and implementation difficulties. The algorithm is designed such that it can detect chaos simultaneously in order to prevent a long time of efficiency decrease.

In Section 2 of this article, a bi-stable energy harvester model is presented using the Euler-Bernoulli beam theory and the assumed mode method. In Section 3, a chaos detection algorithm is presented. The results of chaos detection and noise effect on the algorithm performance are discussed in Section 4. Section 5 concludes the paper.

2. Modeling of bi-stable energy harvester

In this section, an analytical model based on the Euler-Bernoulli beam theory and assumed mode method is presented for a bi-stable energy harvester. The harvester was assumed to be a buckled cantilever Euler-Bernoulli beam with a tip mass, representing the permanent magnet used to create the axial load. All the equations in this section were written according to the previous work [30].

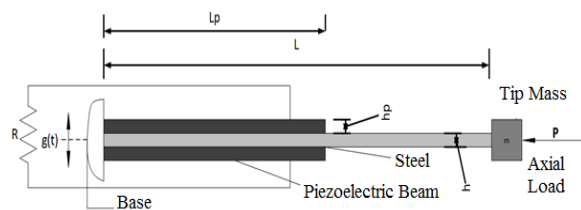


Figure 1. Bi-stable piezoelectric energy harvester.

Table 1. Nomenclature

x_1, x_2, x_3	Geometrical axes along with length, width, and thickness of the beam, respectively.
u_1, u_2, u_3	Displacement of the beam element concerning x_1, x_2, x_3 directions
t	Time
U_b	Elastic potential energy of the beam
S_1	Normal strain in x_1 direction
E	Young's modulus of the beam
\underline{S}	Strain tensor
\underline{T}^b	Beam stress tensor
T_1^b	Beam stress in x_1 direction
A_b	Cross-section area of the beam
I_b	Moment of the cross-section area of the substructure beam
L	Length of the beam
b	Width of the beam and piezoelectric layers
h	Thickness of the beam
h_p	Thickness of each piezoelectric layer
$T_{1,2}^p, T_{1,2}^p$	Stress in piezoelectric layers
c_{11}^e	Young's modulus of the piezoelectric layers
e_{31}	Effective piezoelectric constant
v	Voltage of each piezoelectric layer
U_p	Potential energy of the piezoelectric layers
ϵ_3	Electric field in each piezoelectric layer
A_p	Cross-section area of each piezoelectric layer
Q_p	First moment of inertia of each piezoelectric layer
I_p	Second moment of inertia of each piezoelectric layer
$D_{3,1}, D_{3,2}$	Displacement of electrical load in each piezoelectric layer
ξ_{33}^S	Permittivity of the piezoelectric layer
$\underline{\epsilon}$	Electric field tensor in the piezoelectric layer
g	Base displacement
T	Total kinetic energy
m	Mass of the tip mass
W_{nc}	Work of non-conservative forces
Q	Electrical load crossing the resistive load
P	Axial load
P_s	Axial pressure
W_p	Work of the axial load
x	Dimensionless displacement
η	Dimensionless damping
r	The critical axial load ratio
P	Axial load
k	Linear stiffness
K	Non-linear stiffness
α	Voltage coupling coefficient
λ	Displacement coupling coefficient
χ	Dimensionless time constant
f	Dimensionless amplitude of the external force
Ω	Dimensionless frequency of the external force
τ	Dimensionless time
$\{y\}$	Time-series data
$P(i)$	Series representing reconstructed attractor
τ_1	Reconstruction time delay
$L(t_k)$	Euclidean distance between two nearest neighbors in time t_k
λ_1	Largest Lyapunov exponent (LLE)
N	Number of data in time-series
m	Embedding dimension
M	Number of points on the attractor
σ_d	Standard deviation of the measured data
σ_{noise}	Standard deviation of the noise

Figure 1 shows a schematic representation of the bi-stable piezoelectric energy harvester. As shown in this figure, the bi-stable harvester consists of a clamped steel substructure beam and piezoelectric patches that are connected in series to a resistive

load R. An axial force P is acting to the beam through the permanent magnet with mass m placed at the tip of the beam and the other with opposite poles in the harvester box, not shown in this figure. The whole device is under a base excitation with the displacement of g(t), a pure sine wave with a constant frequency. The displacement field of each element in steel sub-structure beam according to the Euler-Bernoulli beam theory [31] can be written as:

$$u_1 = -x_3 \frac{\partial u_3}{\partial x_1}, u_2 = 0, u_3 = 0 = u_3(x_1, t) \quad (1)$$

where x_1 , x_3 , u_1 , u_3 , and t are the axis in the direction of beam length, perpendicular to the neutral plane, transverse and longitudinal displacements, and time, respectively. According to the Von-Karman strain equation, the only non-zero strain term would be:

$$S_1 = \frac{\partial u_1}{\partial x_1} + \frac{1}{2} \left[\left(\frac{\partial u_1}{\partial x_1} \right)^2 + \left(\frac{\partial u_2}{\partial x_1} \right)^2 + \left(\frac{\partial u_3}{\partial x_1} \right)^2 \right] \\ = -x_3 \frac{\partial^2 u_3}{\partial x_1^2} + \frac{1}{2} \left(\frac{\partial u_3}{\partial x_1} \right)^2 \quad (2)$$

Stress in the substructure beam is:

$$T_1^b = E S_1 = -E x_3 \frac{\partial^2 u_3}{\partial x_1^2} + \frac{1}{2} E \left(\frac{\partial u_3}{\partial x_1} \right)^2 \quad (3)$$

where E is the elastic modulus of the beam. According to equations (2) and (3), the elastic potential energy of the sub-structure beam can be written as:

$$U_b = \frac{1}{2} \iiint_{V_b} \underline{S}^t \underline{T}^b dV_b \\ = \frac{E}{2} \left(I_b \int_0^L \left(\frac{\partial^2 u_3}{\partial x_1^2} \right)^2 dx_1 + \frac{A_b}{4} \int_0^L \left(\frac{\partial u_3}{\partial x_1} \right)^4 dx_1 \right) \quad (4)$$

where S^t is the transpose of the strain matrix and T^b is the stress matrix, V_b is the volume of the substructure beam, A_b is the cross-section area, and I_b is the moment of inertia of the cross-section of the sub-structure beam. According to [30], the stress terms for each piezoelectric plate can be written as:

$$T_{11}^p = c_{11}^\epsilon S_1 - e_{31} \epsilon_3 \\ = -c_{11}^\epsilon x_3 \frac{\partial^2 u_3}{\partial x_1^2} + \frac{c_{11}^\epsilon}{2} \left(\frac{\partial u_3}{\partial x_1} \right)^2 + e_{31} \frac{v}{h_p} \quad (5)$$

$$T_{12}^p = c_{11}^\epsilon S_1 - e_{31} \epsilon_3 = \\ -c_{11}^\epsilon x_3 \frac{\partial^2 u_3}{\partial x_1^2} + \frac{c_{11}^\epsilon}{2} \left(\frac{\partial u_3}{\partial x_1} \right)^2 - e_{31} \frac{v}{h_p} \quad (6)$$

in which e_{31} , c_{11}^ϵ , and v are the effective piezoelectric constant, elastic modulus, and voltage of each piezoelectric plate, respectively. The total elastic potential energy in the piezoelectric plates is:

$$U_p = c_{11}^\epsilon \left(I_p \int_0^{L_1} \left(\frac{\partial^2 u_3}{\partial x_1^2} \right)^2 dx_1 + \frac{A_p}{4} \int_0^{L_1} \left(\frac{\partial u_3}{\partial x_1} \right)^4 dx_1 \right) \\ - e_{31} \frac{v}{h_p} \left(Q_p \int_0^{L_1} \frac{\partial^2 u_3}{\partial x_1^2} dx_1 \right) \quad (7)$$

where:

$$\{A_p, Q_p, I_p\} = b \int_{\frac{h}{2}}^{\frac{h}{2} + h_p} \{1, x_3, x_3^2\} dx_3 \quad (8)$$

The electrical load-displacement in each piezoelectric plate is:

$$D_{31} = e_{31} S_1 + \xi_{33}^\epsilon \epsilon_3 = \\ -e_{31} x_3 \frac{\partial^2 u_3}{\partial x_1^2} + \frac{e_{31}}{2} \left(\frac{\partial u_3}{\partial x_1} \right)^2 - \xi_{33}^\epsilon \frac{v}{h_p} \quad (9)$$

$$D_{32} = e_{31} S_1 + \xi_{33}^\epsilon \epsilon_3 = \\ -e_{31} x_3 \frac{\partial^2 u_3}{\partial x_1^2} + \frac{e_{31}}{2} \left(\frac{\partial u_3}{\partial x_1} \right)^2 + \xi_{33}^\epsilon \frac{v}{h_p} \quad (10)$$

in which ξ_{33}^ϵ is the permittivity of the piezoelectric layer. The total work of the electric field in the piezoelectric layers is:

$$W_e = \frac{1}{2} \iiint_{V_p} \underline{\epsilon}^t \underline{D} dV_p \\ = e_{31} Q_p \int_0^{L_1} \frac{v}{h_p} \frac{\partial^2 u_3}{\partial x_1^2} dx_1 + \xi_{33}^\epsilon A_e \frac{v^2}{h_p} \quad (11)$$

where A_e is the electrode area. The total displacement of every element, according to (1), and base displacement is:

$$\hat{u} = \left\{ -x_3 \frac{\partial u_3}{\partial x_1} \quad 0 \quad u_3(x_1, t) \right\}^T + \{0 \quad 0 \quad g(t)\}^T \quad (12)$$

where g(t) is the base displacement. According to (12), the total kinetic energy of the sub-structure beam, piezoelectric patches, and tip mass is:

$$T = \frac{1}{2} \rho_b A_b \int_0^L \left(\left(\frac{\partial u_3}{\partial t} \right)^2 + \dot{g}^2 + 2 \frac{\partial u_3}{\partial t} \dot{g} \right) dx_1 \\ + \rho_p A_p \int_0^{L_p} \left(\left(\frac{\partial u_3}{\partial t} \right)^2 + \dot{g}^2 + 2 \frac{\partial u_3}{\partial t} \dot{g} \right) dx_1 \\ + \frac{1}{2} m \left(\left(\frac{\partial u_3}{\partial t} + \dot{g} \right) \delta(x_m) \right)^2 \quad (13)$$

where ρ_b and ρ_p are the mass density of the sub-structure beam and piezoelectric layers. The non-conservative work in resistive load is:

$$W_{nc}=2Qv \tag{14}$$

where Q is the electrical load crossing the resistive load. The axial load can be rewritten as:

$$P=P_s(A_b+2A_p) \rightarrow P_s=\frac{P}{A_b+2A_p} \tag{15}$$

Therefore, the work of the axial load is:

$$\begin{aligned} W_p &= \iiint_{V_b} P_s S_1 dV_s + \iiint_{V_p} P_s S_1 dV_p \\ &= \frac{1}{2} \int_0^L P_s A_b \left(\frac{\partial u_3}{\partial x_1}\right)^2 dx_1 \\ &+ \int_0^{L_1} P_s A_p \left(\frac{\partial u_3}{\partial x_1}\right)^2 dx_1 \end{aligned} \tag{16}$$

Utilizing the assumed mode method [31] and Hamilton's law [31], and using (4), (7), (11), (13), (14), and (16), the equations of motion for the single-mode bi-stable energy harvester would be:

$$\begin{aligned} \ddot{x} + \eta \dot{x} + k(1-rP)x + Kx^3 - \alpha v &= f \cos(\Omega\tau) \\ \dot{v} + \lambda \dot{x} + \chi v &= 0 \end{aligned} \tag{17}$$

where $x, \eta, r, P, k, K, \alpha, \lambda, \chi, f, \Omega,$ and τ are the displacement, dimensionless damping of the first mode and dimensionless non-linear stiffness of the first mode, voltage coupling coefficient, displacement coupling coefficient, dimensionless time constant, dimensionless modal force for the first mode, and dimensionless frequency of the excitation and dimensionless time, respectively. The overdots indicate the differentiation concerning time. The variation in the oscillation frequency concerning the axial load is compared with the model of Masana and Daqaq [29] in figure 2. Although the proposed model is much simpler than the model presented by Masana and Daqaq, its prediction of the system dynamics is almost the same as that model.

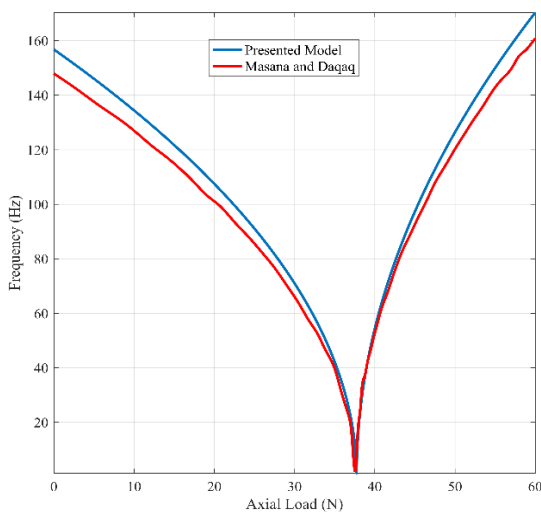


Figure 2. Variation in the frequency of the harvester to the axial load.

In the next sections, the equation sets of (17) are used in order to calculate the bi-stable energy harvester's response and implementation of the chaos detection algorithm.

3. Online estimation of LLE

A chaos detection algorithm based on a new modification of the algorithm of Wolf *et al.* [23] is presented in this section. According to the Taken's embedding theory [32], the attractor can be reconstructed with the embedding dimension of m using a time series consisting of N data points $\{y\}$. The reconstructed attractor can be written as:

$$P(i)=(y_i, y_{i+\tau_1}, y_{i+2\tau_1}, y_{i+3\tau_1}, \dots, y_{i+(m-1)\tau_1}) \tag{18}$$

where τ is the reconstruction delay, and this set represents a point in the attractor in the embedding space. The reconstruction delay can be estimated by the autocorrelation of the time-series data. The time delay is equal to the delay where the autocorrelation data drops to 0.632 of its initial value [25]. After the reconstruction of the attractor using (18), the Euclidean distance, $L(t_0)$, between the nearest neighbor of the initial point $P_{i_0}(i)$ and itself should be calculated. Finding this distance after enough evolution time, let LLE be defined as:

$$\lambda_1 = \frac{1}{t_M - t_0} \sum_{k=0}^M \ln \frac{L(t_k)}{L(t_{k-1})} \tag{19}$$

in which $M=N-(m-1)\tau_1$. First, the whole space of the time-series data will be gridded concerning m and the grid resolution in order to improve the algorithm speed. After gridding the space, the algorithm searches in the nearest boxes to the point rather than the whole data points to find the nearest neighbor. This method will speed up the search procedure. It should be noted that if the distance between two points increases larger than a pre-specified value, the second point will be replaced with the nearest point to the first one in the recent evolution. This procedure will be done for different initial points in the time series, and an average number will be reported as LLE.

To this part, our procedure is almost the same as the conventional procedures of finding LLE using a measured dataset. In the traditional algorithms, the aim is to find the exact value for LLE. However, in controlling the non-linear energy harvesters' chaos, there is only a need to identify the chaotic response. In the algorithm presented here, after gridding the embedding space, instead of working with more than 200,000 data points, only one point and its nearest neighbor in each m -

dimensional box would be randomly chosen in order to calculate LLE rather than using the whole dataset. The sparse matrix calculation can be used with this selection to rapidly calculate the evolution of the distance between two points in time.

The Taken's theory indicates that for an exact reconstruction of the attractor, the embedding dimension, m , should be at least greater than $2 * n$, where n is the fractional dimension of the attractor. In the algorithm presented here, m is considered to be equal to n . With these modifications, one will lose the calculated LLE accuracy but identifying chaos would remain intact. This claim would be addressed in the results and discussion section. The algorithm is designed to calculate LLE of the harvester synchronously. A synchronous detection would give a chance to distinguish between the permanent and temporary chaotic behavior. Controlling chaos would cost energy, and in the case of the temporary chaotic behavior, there is no need to turn the controller on. The harvester's output voltage is considered to be used as the time-series data, and reconstructs the attractor. The next section presents the results and discussion.

4. Results and discussion

4.1. Results of chaos detection

In this section, the harvester's equations of motion are solved using the Runge-Kutta numerical methods, considering the amounts of the harvester geometrical and material properties indicated in table 2.

Table 2. Geometrical and material properties of the harvester.

Name	Symbol	Value
Beam thickness	h_b	0.2 (mm)
Piezoelectric layer thickness	h_p	0.2 (mm)
Beam and piezoelectric width	w_b	25.4 (mm)
Beam length	L	200 (mm)
Piezoelectric layer length	L_p	80 (mm)
Beam's Young's modulus	E	70 (GPa)
piezoelectric layer's Young's modulus	c_{11}^e	60 (GPa)
Resistance of the resistive load	R	450 (KΩ)
Piezoelectric permittivity constant	ξ_{33}^S	25.55 ($\frac{nF}{m}$)
Effective piezoelectric constant	e_{31}	-16.6 ($\frac{C}{m}$)

Figure 2 shows the steady-state time response of the dimensionless voltage considering $\Omega=14$ and $f=0.5$. As it can be seen in this figure, the response is harmonic in the steady-state condition.

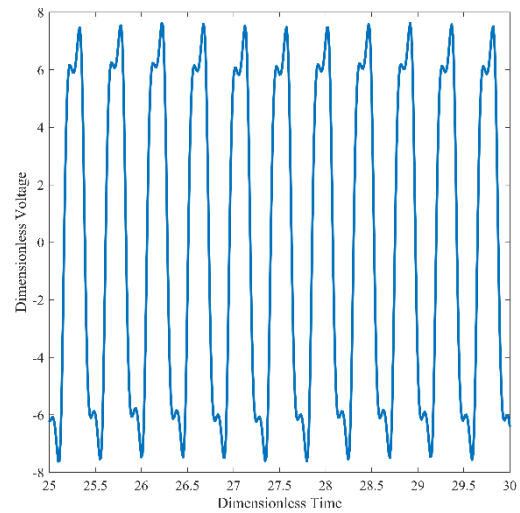


Figure 3. Dimensionless voltage for large amplitude H inter-well oscillation.

Figure 3 shows the estimated LLE for the data presented in figure 2. For estimating LLE, the embedding dimension of $m=4$ and $N=4096$ data points are used in 80 units of dimensionless time. As it can be seen in figure 3, the estimation of LLE is converged after about 100 iterations to zero, which shows the existence of a non-chaotic attractor, i.e. Limit Cycle Oscillations (LCO), which completely meets the oscillations of the system.

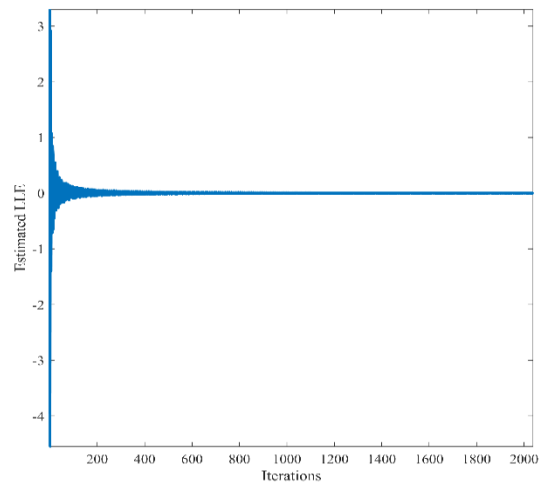


Figure 4. Estimated LLE for harmonic inter-well oscillation.

Setting $f=2.7$ and $\Omega=18$, the system behaves chaotically, as shown in the phase portrait depicted in figure 5. This figure shows the phase space of dimensionless velocity versus dimensionless displacement. The phase space shows the nature of the system response by displaying the orbits of the system response. The depicted orbit is non-periodic and space-limited. It is non-periodic since the orbit does not cover itself, and tends to go over the attractor's whole space. It is space-limited because it does not

exceed the limits of the large amplitude unstable periodic orbit found in this portrait. This type of response indicates a fully chaotic behavior. Figure 6 shows the estimation of LLE for chaotic data in figure 5. This figure shows that the LLE estimation is converged after about 800 iterations, and shows a positive amount indicating a chaotic attractor in the system.

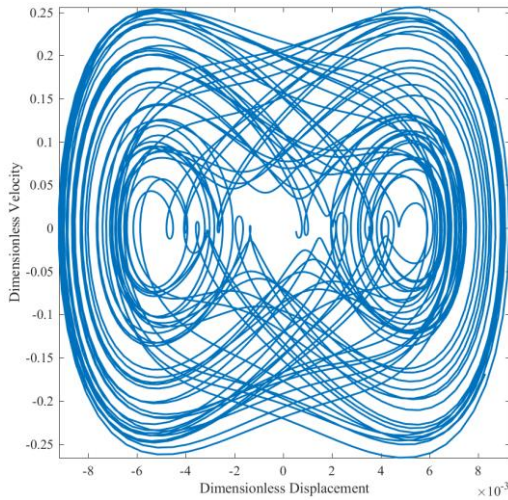


Figure 5. Phase portrait of the bi-stable energy harvester.

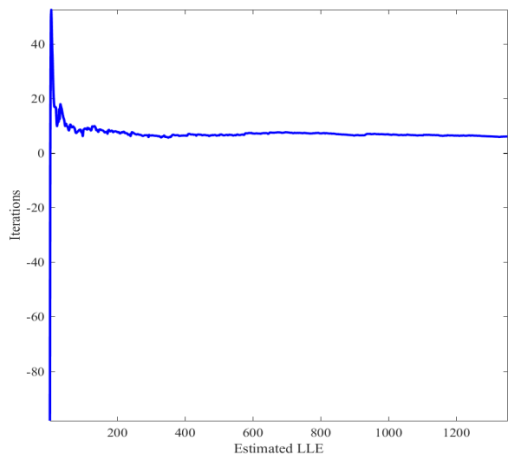


Figure 6. Estimated LLE for chaotic motion.

4.2. Effect of noise

The LLE algorithm is defined to be used on a dataset, which is experimentally measured, in our case, voltage. As it can be expected, the experimentally measured data is always noise-contaminated. Despite using different filtrations and other methods, some noise according to the experimentation circumstances is inevitable. In this section, the effect of noise on the efficiency of the algorithm is presented. In order to define the amount of noise first, the standard deviation of the data is calculated. After that, the noise percentage is selected based on the standard deviations' ratio, as depicted in (21). In (20) and (21), σ_d and σ_{noise}

are the standard deviation of the measured data and added noise, respectively.

$$\{y\} \rightarrow \sigma_d \tag{20}$$

$$\text{noise percentage} = \frac{\sigma_{noise}}{\sigma_d} \cdot 100 \tag{21}$$

Figure 6 shows the voltage response of the system with deliberate noise. These figures show a voltage response of the same simulation contaminated with 10% (a) and 15% (b) of the noise ratio. As the original data has been obtained from the system's periodic response, the algorithm should calculate LLE to be zero.

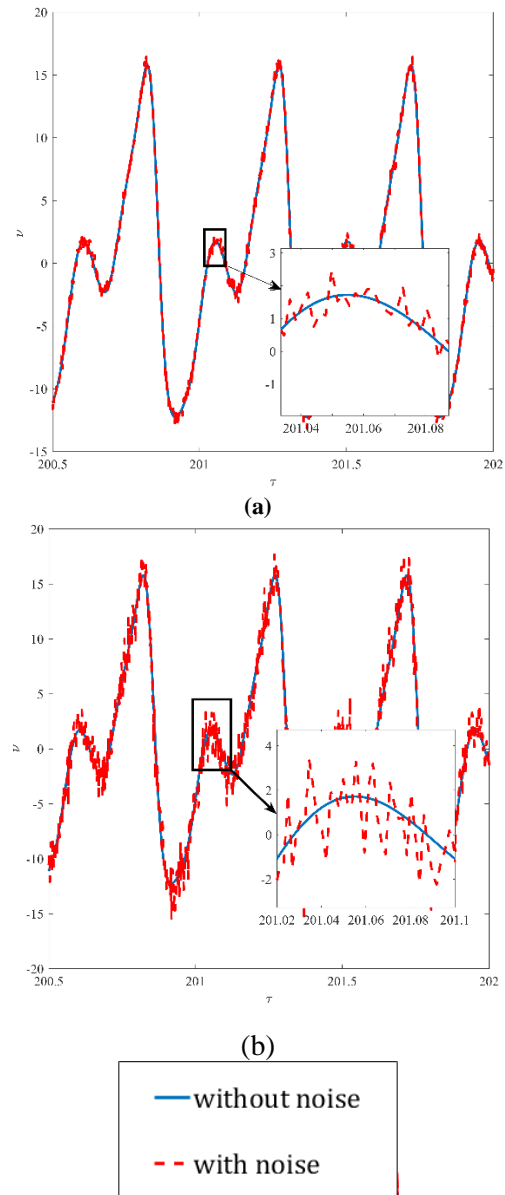
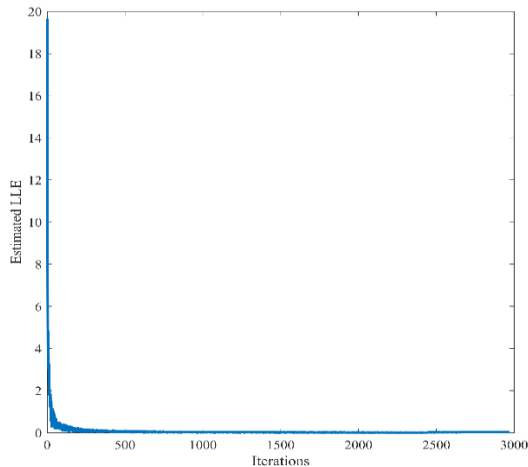


Figure 7. Time response of the voltage with and without noise:

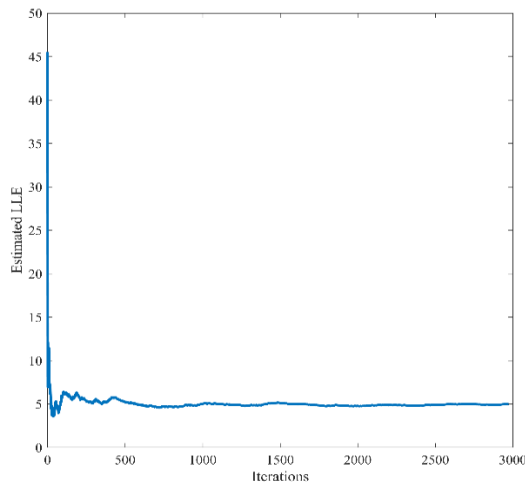
(a) 10% of noise (b) 15% of noise

Figure 7a shows the estimated LLE for the 10% noise ratio. The algorithm can efficiently estimate LLE to be zero, and thus these amounts of noise

do not affect the performance of the chaos detection algorithm. However, as shown in figure 7b, the estimated LLE for the data with a noise ratio of 15% is incorrect. The algorithm fails to distinguish between the real deterministic chaos and the noise. Therefore, the filtration should keep the noise ratio under 15% of the primary data in order to achieve the correct chaos detection.



(a)



(b)

Figure 8. Estimated LLE for data with (a) 10% of noise (b) 15% of noise.

4.3. Comparison with Wolf's algorithm

In this section, the results of the presented algorithm are compared with the classical Wolf's algorithm. Table 2 shows this comparison. As shown in this table, although the algorithm cannot predict LLE as accurate as the Wolf's algorithm, it can successfully distinguish the chaotic and harmonic behaviors even in the presence of noise. The run time of both algorithms is compared in this table. These run times are for the simulation using a corei7 CPU with a frequency of 2 GHz. The proposed algorithm's run time can be significantly lower than the Wolf's algorithm

when the measured data is for a harmonic response, even up to 85%. However, the proposed algorithm has approximately 50 to 60 percent of the Wolf's algorithm's run time for the chaotic data.

Table 3. Comparison of the performance of MWM with the Wolf's algorithm.

Algorithm		Signal type			
		Harmonic	Noisy harmonic	Chaotic	Noisy chaotic
Wolf	LLE	$1.2e - 5$	$2.7e - 2$	2.06	1.82
	Result	Harmonic	Harmonic	Chaotic	Chaotic
	Run Time (s)	27.2	36.7	48.1	53.1
MWM	LLE	$-9e - 3$	$3.6e - 2$	2.1	2.55
	Result	Harmonic	Harmonic	Chaotic	Chaotic
	Run Time (s)	5.2	4.9	23.6	32.2

5. Conclusion

In this work, a new simple model based on the Euler-Bernoulli beam theory and the Von-Karman strain for axially loaded non-linear vibration energy harvesters was derived. The model was validated by comparing the frequency-load curve with the model of Masana and Daqaq [29]. A new modification of the Wolf's method [23] and the Rosenstein's algorithm [25] was derived. The proposed algorithm was used to identify the harvester's chaotic and harmonic responses using the time-series data of the output voltage calculated by the numerical method. Accordingly, the algorithm had the merit of using only one sensor in the experimental implementation. The findings of this work could be summarized as follow:

1. The proposed model had excellent predictions on the response of the system.
2. The chaos detection algorithm could successfully identify the chaotic and harmonic responses.
3. The algorithm could detect chaos for noisy data having up to 10% of noise density.
4. The algorithm was much faster than the primary Wolf's method, and it could be faster up to 85%

This work showed that the algorithm could be used in the control system of the bi-stable energy harvesters.

6. Acknowledgment

The authors of this article are grateful to the Renewable Energies Engineering Laboratory of the Shahid Beheshti University for their support and for providing the necessary equipment.

7. References

- [1] G. Rsr, K. Pallikonda, and G. Walunj, "Use of Rayleigh Distribution Method for Assessment of Wind Energy Output in Cleveland-Ohio," *Renew. Energy Res. Appl.*, Vol. 1, No. 1, pp. 11–18, 2020.
- [2] M. L. Kamari, H. Isvand, and M. A. Nazari, "Applications of Multi-Criteria Decision-Making (MCDM) Methods in Renewable Energy Development: A Review," *Renew. Energy Res. Appl.*, Vol. 1, No. 1, pp. 47–54, 2020.
- [3] F. Narita and M. Fox, "A Review on Piezoelectric, Magnetostrictive, and Magnetoelectric Materials and Device Technologies for Energy Harvesting Applications," *Adv. Eng. Mater.*, Vol. 20, No. 5, pp. 1–22, 2018.
- [4] M. F. Daqaq, R. Masana, A. Erturk, and D. Dane Quinn, "On the Role of Nonlinearities in Vibratory Energy Harvesting: A Critical Review and Discussion," *Appl. Mech. Rev.*, Vol. 66, No. 4, p. 040801, 2014.
- [5] Y. Jia, "Review of non-linear vibration energy harvesting: Duffing, bistability, parametric, stochastic and others," *J. Intell. Mater. Syst. Struct.*, vol. 31, No. 7, pp. 921–944, 2020.
- [6] R. Masana and M. F. Daqaq, "Relative performance of a vibratory energy harvester in mono- and bi-stable potentials," *J. Sound Vib.*, Vol. 330, No. 24, pp. 6036–6052, 2011.
- [7] M. Panyam and M. F. Daqaq, "A comparative performance analysis of electrically optimized non-linear energy harvesters," *J. Intell. Mater. Syst. Struct.*, Vol. 27, No. 4, pp. 537–548, 2016.
- [8] R. Naseer, A. Abdelkefi, H. Dai, and L. Wang, "Characteristics and comparative analysis of mono-stable and bistable piezomagnetoelastic energy harvesters under vortex-induced vibrations," 2018 AIAA/ASCE/AHS/ASC Struct. Struct. Dyn. Mater. Conf., No. January pp. 1–9, 2018.
- [9] R. L. Harne and K. W. Wang, "A review of the recent research on vibration energy harvesting via bistable systems," *Smart Mater. Struct.*, Vol. 22, No. 2, p. 023001, 2013.
- [10] Q. He and M. F. Daqaq, "New Insights Into Utilizing Bistability for Energy Harvesting Under White Noise," *J. Vib. Acoust.*, Vol. 137, No. 2, p. 021009, 2015.
- [11] C. R. McInnes, D. G. Gorman, and M. P. Cartmell, "Enhanced vibrational energy harvesting using non-linear stochastic resonance," *J. Sound Vib.*, Vol. 318, No. 4–5, pp. 655–662, 2008.
- [12] F. Cottone, H. Vocca, and L. Gammaitoni, "Nonlinear Energy Harvesting," Vol. 080601, No. February pp. 1–4, 2009.
- [13] B. P. Mann and B. A. Owens, "Investigations of a non-linear energy harvester with a bistable potential well," *J. Sound Vib.*, Vol. 329, No. 9, pp. 1215–1226, 2010.
- [14] S. C. Stanton, B. A. M. Owens, and B. P. Mann, "Harmonic balance analysis of the bistable piezoelectric inertial generator," *J. Sound Vib.*, Vol. 331, No. 15, pp. 3617–3627, 2012.
- [15] M. Panyam, R. Masana, and M. F. Daqaq, "On approximating the effective bandwidth of bi-stable energy harvesters," *Int. J. Non. Linear. Mech.*, Vol. 67, pp. 153–163, 2014.
- [16] A. Kumar, S. F. Ali, and A. Arockiarajan, "Enhanced energy harvesting from non-linear oscillators via chaos control," *IFAC-PapersOnLine*, Vol. 49, No. 1, pp. 35–40, 2016.
- [17] B. H. Huynh, T. Tjahjowidodo, Z.-W. Zhong, Y. Wang, and N. Srikanth, "Design and experiment of controlled bistable vortex-induced vibration energy harvesting systems operating in chaotic regions," *Mech. Syst. Signal Process.*, Vol. 98, pp. 1097–1115, 2018.
- [18] A. Yousefpour, A. Haji Hosseinloo, M. Reza Hairi Yazdi, and A. Bahrami, "Disturbance observer-based terminal sliding mode control for the effective performance of a non-linear vibration energy harvester," *J. Intell. Mater. Syst. Struct.*, Vol. 31, No. 12, pp. 1495–1510, 2020.
- [19] E. Ott, C. Grebogi, and J. A. Yorke, "Controlling chaos," *Phys. Rev. Lett.*, Vol. 64, No. 11, pp. 1196–1199, 1990.
- [20] H. G. Schuster, U. Parlitz, and L. Kocarev, *Handbook of Chaos Control*. Wiley-VCH Verlag GmbH & Co.KGaA, 2008.
- [21] A. Haji Hosseinloo, J.-J. Slotine, and K. Turitsyn, "Robust and adaptive control of coexisting attractors in non-linear vibratory energy harvesters," *J. Vib. Control*, No. November 2016, p. 107754631668899, 2017.
- [22] P. Harris, C. R. Bowen, H. A. Kim, and G. Litak, "Dynamics of a vibrational energy harvester with a bistable beam: Voltage response identification by multiscale entropy and '0-1' test," *Eur. Phys. J. Plus*, Vol. 131, No. 4, 2016.
- [23] A. Wolf, "Estimating the dominant Lyapunov exponent from a Time Series Documentation for the efficient version of the algorithm of Wolf et al.," pp. 1–25, 1985.
- [24] S. Kodba, M. Perc, and M. Marshall, "Detecting chaos from a time series," *Eur. J. Phys.*, Vol. 26, No. 1, pp. 205–215, 2005.
- [25] Michael T. Rosenstein James J. Collins, C. J. De Luca, M. T. Rosenstein, J. J. Collins, and C. J. De Luca, "A practical method for calculating largest

Lyapunov exponents from small data sets," *Phys. D Nonlinear Phenom.*, Vol. 65, No. 1–2, pp. 117–134, 1993.

[26] S. Zhou, X. Wang, Z. Wang, and C. Zhang, "A novel method based on the pseudo-orbits to calculate the largest Lyapunov exponent from chaotic equations," *chaos*, Vol. 29, No. 3, 2019.

[27] S. Zhou and X. Wang, "Simple estimation method for the largest Lyapunov exponent of continuous fractional-order differential equations," *Phys. A Stat. Mech. its Appl.*, Vol. 563, p. 125478, 2021.

[28] S. Mehdizadeh, "A robust method to estimate the largest Lyapunov exponent of noisy signals: A revision to the Rosenstein's algorithm," *J. Biomech.*, Vol. 85, pp. 84–91, 2019.

[29] R. Masana and M. F. Daqaq, "Electro-mechanical Modeling and non-linear analysis of axially loaded energy harvesters," *J. Vib. Acoust. Trans. ASME*, Vol. 133, No. 1, 2011.

[30] M. Mohammadpour, M. Dardel, and M. H. Ghasemi, "Non-linear energy harvesting through a multimodal electro-mechanical system," *J. Theor. Appl. Vib. Acoust. - TAVA*, Vol. 1, No. 2, pp. 73–84, 2015.

[31] S. S. Rao, *Vibration of Continuous Systems* (2007). 2007.

[32] L. NOAKES, "the Takens Embedding Theorem," *Int. J. Bifurc. Chaos*, Vol. 01, No. 04, pp. 867–872, 1991.